2012-07

Estimation of Human Foot Motion During Normal Walking Using Inertial and Magnetic Sensor Measurements

Yun, Xiaoping; Calusdian, James; Bachmann, Eric R.; McGhee, Robert B.

IEEE

Yun, Xiaoping, et al. "Estimation of human foot motion during normal walking using inertial and magnetic sensor measurements." IEEE transactions on Instrumentation and Measurement 61.7 (2012): 2059-2072.
http://hdl.handle.net/10945/63773

Estimation of Human Foot Motion During Normal Walking Using Inertial and Magnetic Sensor Measurements

Xiaoping Yun, *Fellow, IEEE*, James Calusdian, Eric R. Bachmann, *Member, IEEE*, and Robert B. McGhee, *Life Fellow, IEEE*

***Abstract*—A foot motion filtering algorithm is presented for estimating foot kinematics relative to an earth-fixed reference frame during normal walking motion. Algorithm input data are obtained from a foot-mounted inertial/magnetic measurement unit. The sensor unit contains a three-axis accelerometer, a three-axis angular rate sensor, and a three-axis magnetometer. The algorithm outputs are the foot kinematic parameters, which include foot orientation, position, velocity, acceleration, and gait phase. The foot motion filtering algorithm incorporates novel methods for orientation estimation, gait detection, and position estimation. Accurate foot orientation estimates are obtained during both static and dynamic motion using an adaptive-gain complementary filter. Reliable gait detection is accomplished using a simple finite state machine that transitions between states based on angular rate measurements. Accurate position estimates are obtained by integrating acceleration data, which has been corrected for drift using zero velocity updates. Algorithm performance is examined using both simulations and real-world experiments. The simulations include a simple but effective model of the human gait cycle. The simulation and experimental results indicate that a position estimation error of less than 1% of the total distance traveled is achievable using commonly available commercial sensor modules.**

***Index Terms*—Accelerometers, angular rate sensors, complementary filter, foot kinematics, foot motion, gyros, inertial sensors, magnetic sensors, personal navigation, position estimation.**

I. Introduction

NUMEROUS applications require a self-contained personal navigation system that works in indoor and outdoor environments, does not require any infrastructure support, and is not susceptible to interference. Position tracking of human movement commonly requires an unrestricted line-of-sight to an installed infrastructure consisting of one or more transmitters and/or receivers. Such systems require extensive setup and calibration of the tracking volume, which may be of limited size and may suffer from occlusion. Examples of this type of tracking are generally based on radio frequency, such as GPS, or may use optical-based systems, such as video tracking.

Manuscript received July 11, 2011; revised October 26, 2011; accepted October 28, 2011. Date of publication January 31, 2012; date of current version June 8, 2012. This work was supported in part by the National Science Foundation (NSF) and the Army Research Office (ARO). The Associate Editor coordinating the review process for this paper was Dr. Kurt Barbe.

The authors are with the Naval Postgraduate School, Monterey, CA 93943 USA.

Color versions of one or more of the figures in this paper are available online at http://ieeexplore.ieee.org.

Digital Object Identifier 10.1109/TIM.2011.2179830

Alternatively, a self-contained tracking system using small inertial/magnetic measurement units (IMMUs) will not have limitations due to occlusions in the covered tracking space. Applications using commercially available IMMUs containing triads of orthogonally mounted accelerometers, angular rate sensors, and magnetometers have been successfully demonstrated. See for example [1]–[3]. Several commercial orientation tracking systems are currently in the market. Commercial examples of such IMMUs include the InterSense InertiaCube 2+ [4], the Xsens MTx [5], the MicroStrain 3DM-GX3-25 [6], and the MEMSense nIMU [7]. The individual inertial sensors used in IMMUs are low-cost, low-power, and lightweight based on microelectromechanical systems (MEMS) technology.

However, the performance of MEMS accelerometers and angular rate sensors is limited by random noise and calibration error. Magnetometer accuracy is affected by hard-iron and soft-iron interference. Consequently, when the IMMU is used in a position tracking system, it becomes the source of unbounded growth in position error. Novel and innovative methods have been proposed by many researchers to address the limitations inherent in the commercial IMMU.

Much research has focused on using inertial sensors in combination with magnetic sensors to measure distance walked and/or to track position. In the available body of research, two main approaches to position tracking are identified. One method is based on counting steps and estimating distance based on an approximate step length, with some researchers reporting good results [8]–[13]. This technique circumvents the growth in position error that arises from the double integration of acceleration but may be limited by the accuracy in which the step length can be determined and the general heading of the body. The other main approach is an adaptation of the well-known strapdown navigation algorithm, which incorporates double integration of the measured acceleration to estimate distance and or position. The work described here is based on this latter approach.

In this and in similar work by other researchers, the growth in position uncertainty that arises from the integration of the acceleration error is mitigated by a technique that is commonly referred to as zero-velocity updates (ZVUs) [14]. Most types of human movement, such as walking, side stepping, and running, have repeated recognizable periods during which the velocity and acceleration of the foot are zero. These brief periods occur before entering the swing phase of the gait cycle each time the

Fig. 1. Depiction of an inertial/magnetic sensor module attached to a foot for tracking foot motion during normal walking.

foot contacts the ground during the stance phase. The use of a foot-mounted IMMU, as shown in Fig. 1, provides sensor data for recognition of these periods. This provides a means to determine the drift error and to facilitate correction to the velocity in preparation for subsequent integration to derive position. Since this correction is applied at the end of every walking step, it provides a type of immediate recalibration of the sensor.

Some previous works that utilized the ZVU technique include Sagawa *et al.* [15], Sabatini *et al.* [16], and Cavallo *et al.* [17]. These researchers used a combination of accelerometers and rate sensors attached to the foot to measure gait parameters and distance traveled. The Sagawa approach used a tri-axial accelerometer and a single axis angular rate sensor attached to the toe (an atmospheric pressure sensor is used to measure change in altitude). The Sabatini and Cavallo approaches used a bi-axial accelerometer and a single axis angular rate sensor attached to the instep.

Sagawa *et al.* assumed that foot roll and yaw are zero during normal walking [15]. Sabatini *et al.* [16] assumed that all motion takes place in a sagittal plane. In both cases, a rate sensor was mounted perpendicular to the sagittal plane. Gait events such as heel-off, heel-strike, and swing, were detected using angular rate sensor data. Instead of counting steps, walking speed and stride length were estimated by double integration of accelerometer data. For best performance, the tracked subject was required to maintain a uniform walking speed and gait. Both research efforts were able to detect gait events with high levels of confidence. In limited experimental results, Sagawa *et al.* reported a maximum distance estimation error of 5.3% over a 30-m course. Experimental results obtained while walking over a 400-m closed course reported a smaller error, with an average measured distance of 401.2 ± 4.61 m or just over a 1% error. Although GPS heading information was used in [17] to reconstruct the path of travel, neither of the systems described was able to determine the direction of displacement or position. In [18], Sabatini described a quaternion-based extended Kalman filter for determining the orientation of a rigid body, which is applicable to tracking human movement.

The commercial availability of the IMMU has improved in recent years, and newer IMMUs have expanded to include triads of orthogonally mounted accelerometers, angular rate sensors, and magnetometers that are integrated into lightweight miniature packages. Because of this, more recent work has shown the promise of using the IMMU in the tracking of foot motion and for the determination of position.

In [19], Foxlin used a foot-mounted IMMU from InterSense incorporating the ZVU and an extended Kalman filter to achieve error performance on the order of 0.3% of distance walked using a magnetometer that has been recently calibrated. In another work by Ojeda and Borenstein [20], error on the order of 2% of distance walked was reported. A noteworthy aspect of their work was the incorporation of additional corrections in the calibration of the accelerometers and angular rate sensors to account for temperature variation and random variation. Furthermore, their results were achieved exclusive of the magnetometers available within the IMMU that was utilized. In a recent work by Bebek *et al.* [21], a position error of less than 1% was reported. This work incorporated an additional calibration based on the total drift that accumulated during an initial walk. This information was used to correct subsequent walks to produce desirable results.

Since these works were based on the ZVU, it was necessary to identify the instances of swing phase and stance phase with a high degree of accuracy. Some researchers have developed specific electronic circuits to aid in the detection of the foot stance phase. For example, in [22], a shoe-mounted radar was developed to detect the instances of the foot zero velocity. Others have incorporated force-sensitive resistors into the shoe or foot-mounted switches, such as in [21], [23], and [24]. While this approach yields very accurate results, it does introduce an added level of complexity to the overall system.

This paper describes a self-contained method for estimating the kinematics of the human foot during normal walking motion. In this paper, normal walking refers to forward walking of a healthy person as opposed to backward walking, sidestepping, Nordic walking, hopping, skipping, jumping, running, etc. The method is based on the use of IMMUs attached to the foot. The primary contributions of this paper are the following.

1) An adaptive-gain complementary filter designed to accurately estimate orientation during both static and dynamic motion. While the filter described is useful in many applications, it is particularly suited for determination of foot orientation during static stance phases and dynamic swing phases.
2) A reliable gait detection method requiring only input from foot-mounted angular rate sensors. The method consists of a two-state finite state machine, which tracks the stance and swing phases of the human gait cycle.
3) A method for accurate position estimation by integrating acceleration data that have been corrected for drift using ZVUs.
4) Simulation and real-world experimental results, which indicate that the aforementioned methods are accurate and have practical applications.

The remainder of this paper presents in detail the foot motion filtering algorithm and experimental results. Section II describes the foot motion filtering algorithm and includes a separate section for each of the major components. Section III describes a simulation framework for evaluating the foot motion filtering algorithm and for isolating and quantifying the

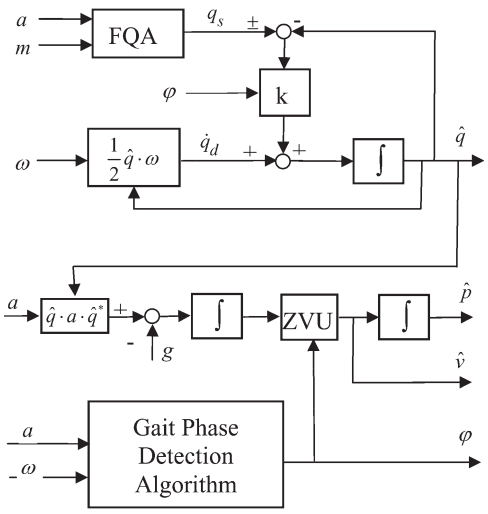

Fig. 2. Block diagram of the foot motion tracking algorithm that produces the foot orientation quaternion, foot position, foot velocity, and gait phase.

various sources of error. Discussion and results pertaining to simulation studies and real-world experiments are presented in Section IV. The final section summarizes the conclusion that can be drawn from this paper.

II. Foot Motion Filtering Algorithm

This section presents a motion filtering algorithm based on the use of a foot-mounted IMMU. A block diagram of the foot motion filtering algorithm is shown in Fig. 2. The upper, middle, and lower portions of the diagram correspond to the three main components of the algorithm. The upper portion of the diagram depicts the adaptive-gain quaternion-based complementary filter for estimating foot orientation represented by a quaternion $\hat{q}$ from the acceleration measurement a, the local magnetic field measurement m, and the angular rate measurement ω. The middle portion of the diagram depicts the position and velocity estimation filter. The outputs are the foot velocity estimate $\hat{v}$ and the foot position estimate $\hat{p}$. The lower portion of the diagram shows the gait phase detection algorithm. At any given moment, the gait phase, denoted by φ, will have one of two values, which correspond to the swing or stance phases of the normal walking cycle. Each of the main components of the filter algorithm is described in detail in the following sections.

A. Adaptive-Gain Quaternion-Based Complementary Filter for Orientation Estimation

The upper portion of Fig. 2 shows a complementary filter for estimating orientation of a foot or any other object to which an inertial/magnetic sensor module is attached. The input to this filter is nine components of the inertial/magnetic sensor measurements, which are three components of the accelerometer measurement a, three components of the local magnetic field measurement m, and three components of the angular rate measurement ω. The output of the filter is the estimated foot orientation represented by a quaternion $\hat{q}$. All measurements provided by the IMMU are represented in the sensor or body coordinate system. To differentiate the same quantity in the body coordinate system or the earth coordinate system, a superscript is used to indicate the coordinate system. For example

$$a^b = \begin{bmatrix} a_x^b \\ a_y^b \\ a_z^b \end{bmatrix} \tag{1}$$

denotes the acceleration and its three components in the body coordinate system.

The algorithm designed for orientation estimation is a type of filter that blends two sources of data in a complementary manner [25]. In this case, the filter blends the static low-frequency information provided by accelerometers and magnetometers, and the dynamic high-frequency information provided by the angular rate sensors. If the foot or any other body to which the inertial/magnetic sensor module is attached is stationary or moving slowly, measurements provided by accelerometers and magnetometers are sufficient to estimate the body orientation accurately [26]. Thus, measurements from these sensors can be heavily weighted in the filter. However, if the body is subject to movement with relatively large linear accelerations, this component cannot be separated from the gravitational acceleration, and the orientation estimate becomes less accurate. In this case, angular rate measurements are more heavily weighted relative to accelerometer measurements for orientation estimation.

The complementary filter has two branches: the static quaternion branch q_s and the dynamic quaternion branch q_d. The static quaternion q_s is computed using the factored quaternion algorithm (FQA). The FQA is a method of estimating the orientation of a static or slow-moving rigid body based on accelerometer and magnetometer measurements. In the algorithm, the measured acceleration and local magnetic field vectors are used to estimate orientation without memory effect. Magnetometer measurements are used only to determine orientation within the horizontal plane [26]. In the dynamic branch, a quaternion rate $\dot{q}_d$ is computed from the angular rate measurement ω and the most recent quaternion estimate $\hat{q}$ using the well-known quaternion equation [27]

$$\dot{q}_d = \frac{1}{2}\hat{q}\cdot\omega \tag{2}$$

where the product between $\hat{q}$ and ω is quaternion multiplication and the measured angular rate ω is expressed as a pure vector quaternion with the scalar part equal to zero and the vector part corresponding to the measured components of the angular rate vector for the body coordinate x, y, and z axes.

The filter gain k has the effect of adjusting the relative weight of the two branches. The static quaternion q_s produced by the FQA is compared with the most recent orientation estimate of the complementary filter $\hat{q}$ to produce a quaternion error $e(t) = \pm q_s(t) - \hat{q}(t)$. The $\pm$ in front of $q_s(t)$ is used to indicate that a quaternion having the same sign as $\hat{q}(t)$ must be used here. The quaternion error $e(t)$ is multiplied by the feedback gain k, which is then added to $\dot{q}_d(t)$ in order to produce a corrected dynamic quaternion rate. The corrected quaternion rate is finally integrated to yield the estimated quaternion. Although

not shown in Fig. 2, the estimated quaternion is immediately normalized to ensure that it remains a unit quaternion.

The complementary nature of the orientation filter can be analyzed using the Laplace transform. Applying the principle of superposition and assuming that the input to the dynamic branch is zero, the transfer function from the static quaternion $Q_s(s) = \mathcal{L}\{q_s(t)\}$ to the estimated output quaternion $\hat{Q}(s) = \mathcal{L}\{\hat{q}(t)\}$ is given by

$$H_s(s) = \frac{\hat{Q}(s)}{Q_s(s)} = \frac{k}{s+k}. \tag{3}$$

Now assuming that the input to the static branch is zero, the transfer function for the dynamic branch is

$$H_d(s) = \frac{\hat{Q}(s)}{Q_d(s)} = \frac{s}{s+k}. \tag{4}$$

Equation (3) is a first-order low-pass filter with the corner frequency at $\omega_c = k$ and a unit gain at very low or dc frequencies. On the other hand, (4) is a first-order high-pass filter with the same corner frequency $\omega_c = k$. Thus, at lower frequencies, the filter output relies more on the static quaternion $q_s(t)$ computed by FQA with acceleration and local magnetic field measurements as input. At higher frequencies, the filter output relies more on the dynamic information provided by the angular rate measurements. At or near the corner frequency, the filter output is a fusion of both static and dynamic information [28].

The corner frequency is determined by the choice of the filter gain k. The optimal value of the filter gain depends on the application or motion to which the sensor module is subjected. In general, if the sensor module is subjected to relatively slow movements, a larger feedback gain is preferred. Conversely, if the sensor module undergoes relatively fast motion, a smaller feedback gain is chosen.

To accurately track foot motion during normal walking, an adaptive-gain strategy can be adopted. As shown in Fig. 2, the value of the filter gain k is affected by the gait phase φ, which is computed by the gait phase detection algorithm at the lower portion of Fig. 2. Here, the state of the gait is characterized as either the stance phase or the swing phase. During the stance phase, the foot is in contact with the ground and has zero or a relatively small angular velocity. A larger filter gain is used during the stance phase. During the swing phase, the foot is in motion, and a smaller value for the filter gain is used.

B. Position and Velocity Estimation Filter With ZVU

The middle portion of Fig. 2 shows the position and velocity estimation filter. The input to this filter is the measured acceleration vector in the body coordinates, and the output is the estimated position $\hat{p}(t)$ and velocity $\hat{v}(t)$ relative to a fixed earth coordinate frame. This filter uses the estimated quaternion $\hat{q}(t)$ generated by the complementary orientation filter, which is shown in the upper portion of Fig. 2, to transform acceleration measurements from the body coordinates to earth coordinates.

The input to the position and velocity estimation filter is the measured acceleration vector a^b in the body coordinate system, which is simply shown as a in Fig. 2 for brevity. This is the same measurement vector used by the FQA. The first step of the position and velocity estimation filter is to transform the body coordinate acceleration into the earth coordinate system using the quaternion operator

$$a^e(t) = \hat{q}(t) \cdot a^b(t) \cdot \hat{q}^*(t) \tag{5}$$

where $\hat{q}(t)$ is the estimated quaternion representing the orientation of the body, $\hat{q}^*(t)$ is the quaternion conjugate, and the product in the equation is quaternion multiplication. The acceleration vectors $a^b(t)$ and $a^e(t)$ are treated as pure vector quaternions, with the scalar part being equal to zero when performing quaternion multiplication. After obtaining the acceleration vector $a^e(t)$ in the earth coordinate system, gravitational acceleration g^e is subtracted from $a^e(t)$ to derive the motion-induced acceleration

$$a^e_m(t) = a^e(t) - g^e. \tag{6}$$

The result of (6) is integrated to obtain the 3-D velocity vector in the earth coordinate system

$$v^e_m(t) = \int a^e_m(t)\, dt. \tag{7}$$

Theoretically, the velocity vector resulted from (7) can be immediately integrated once again to obtain position. However, due to the presence of measurement noise and drift in the measured acceleration vector $a^b(t)$ and the estimation errors in the estimated quaternion $\hat{q}(t)$, an immediate integration of $v^e_m(t)$ results in unbounded error growth in position estimation in a relatively short time.

An approach to reduce error growth in the position estimation is to apply a velocity correction method called the ZVU. The concept of the ZVU is based on the observation that human foot motions are cyclic, and when a foot is in the stance phase or in contact with the ground, its velocity is zero. Due to bias error in acceleration measurements, the estimated foot velocity obtained from (7) may not be zero while the foot is in the stance phase. The difference between the actual velocity, which is known to be zero, and the velocity derived through integration is used to correct for the acceleration bias error. Specifically, the acceleration measurement $a^e_m(t)$ of a foot over a period of the swing phase is considered to be in the form of

$$a^e_m(t) = a^e_a(t) + \varepsilon, \qquad t \in [0,\ T] \tag{8}$$

where $a^e_a(t)$ is the actual or true acceleration, ε is the bias error, and T is the duration of the swing phase. Over the short period of the swing phase, the bias error ε may be assumed to be constant. The foot velocity at the beginning of the swing phase is zero. The foot velocity during the swing phase is computed using (7)

$$\begin{aligned} v^e_m(t) &= \int_0^t a^e_m(\tau) d\tau = \int_0^t \left[a^e_a(\tau) + \varepsilon\right] d\tau \\ &= \int_0^t a^e_a(\tau) d\tau + \int_0^t \varepsilon d\tau = v^e_a(t) + \varepsilon t. \end{aligned} \tag{9}$$

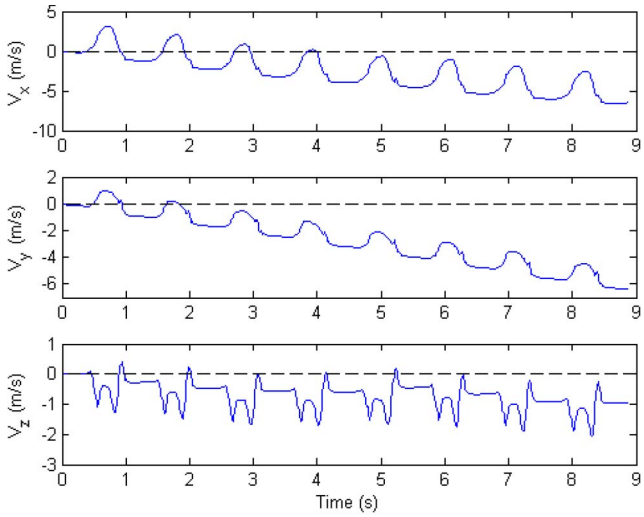

Fig. 3. Three-axis foot velocity prior to applying the ZVU.

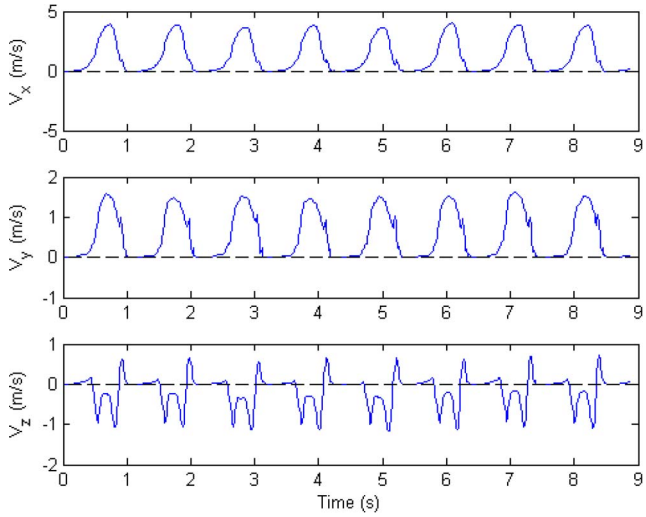

Fig. 4. Three-axis foot velocity after applying the ZVU.

The computed velocity $v_m^e(t)$ is composed of two parts. The first part $v_a^e(t)$ is the actual or true velocity, and the second part εt is due to bias error. At the end of the swing phase when $t = T$, the foot is again in contact with the ground, and the actual velocity is known to be zero. As a result, the bias error in the acceleration measurement can be estimated by

$$\varepsilon = \frac{v_m^e(T)}{T}. \tag{10}$$

This acceleration bias error estimate can now be used to correct velocity and position estimate during the swing phase. Fig. 3 shows the three-axis foot velocity prior to applying the ZVU. The presence of drift is evident in all three components of velocity. Moreover, the drift in the velocity appears to be linear, which confirms the assumption that the acceleration bias is constant over the short period of a swing phase. Fig. 4 shows the same velocity after applying the ZVU. It is seen that the corrected foot velocity during the stance phase is now zero. This corrected velocity, denoted by $\hat{v}$ in Fig. 2, is integrated again to obtain the estimated position $\hat{p}$. It is noted that all sensor measurements and position/velocity vectors are 3-D in this paper. Thus, the filter described previously estimates 3-D position and velocity.

C. Gait Phase Detection Algorithm

To utilize the ZVU for correcting foot velocity, it is necessary to accurately detect the stance and swing phases of foot motion. The use of both accelerometer and angular rate data was examined for this purpose. Initially, the foot acceleration seemed to provide a means for the detection of the transitions between the stance phase and swing phase. After further experiment, however, the angular rate of the foot was found to be more reliable in discriminating the periods of the swing and stance phase motions. Only the use of angular rate data is discussed here. For a discussion on the use of accelerometers to detect the gait phases, see [29]. A thorough analysis of gait detection techniques is found in [30].

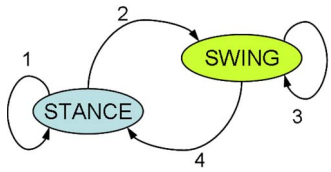

Fig. 5. State machine describing the operation of the gait phase detection algorithm.

The gait phase detection algorithm is essentially a state machine with two states—STANCE and SWING. Fig. 5 shows the two states of the gait phase detection algorithm and the allowed transitions between them. The operation of the state machine must be synchronized with the user's foot motion. That is, when the user's foot was in the stance phase, the state machine must be in this state. Conversely, when the user's foot is in the swing phase, the state machine should reflect this state as well.

Generally speaking, the angular rate measurements are zero or relatively small when the foot is in the stance phase. However, a close examination of the typical angular rate measurements during normal walking reveals that the angular rates may momentarily dip to small values during the swing phase. As such, a simple threshold algorithm is not sufficient to accurately detect the gait phases. To circumvent this problem, a timer, as well as a threshold, was utilized. The state machine will transition between states only when the angular rate has been above or below the threshold for a specified time period. In this way, momentary dips and sudden spikes in the angular rate measurements are filtered out.

Based on the aforementioned discussion, two parameters were monitored during the execution of the algorithm. The first was the magnitude of the angular rate measurements $|\omega|$. It was compared against a threshold value Ω_{th}. The second parameter was a sample count γ that was incremented until a specified number of samples had satisfied the minimum count condition. Fig. 6 shows $|\omega|$ identified as the angular rate length on the vertical axis of the plot, as well as the output of the gait phase detection algorithm, shown in blue and red, respectively. The value of the threshold Ω_{th} is identified on the plot. Examination

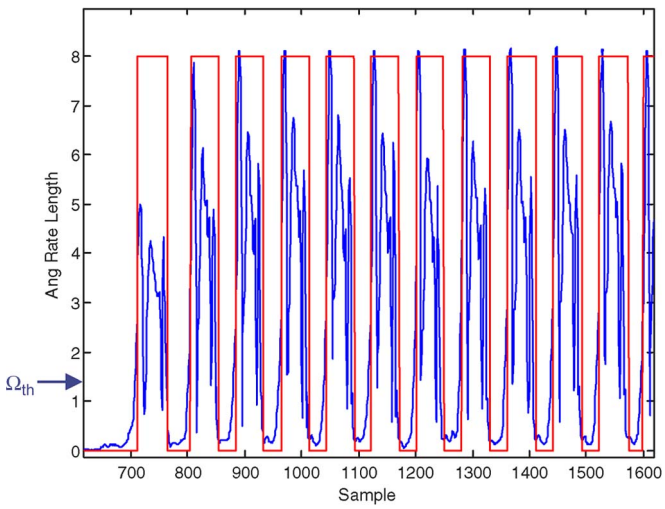

Fig. 6. Angular rate length (blue) and the stance/swing phases (red).

of the plot shows that the gait phase detection algorithm accurately locates the periods of the swing and stance phases.

D. Implementation Considerations for the ZVU and Gait Phase Detection Algorithm

The operation of the gait phase detection algorithm is based on proper selection of two threshold parameters Ω_{th} and Γ_{th}, where the latter of which is compared with the sample count γ during each iteration of the code. As a result of this, the moment that the algorithm changes state will be delayed from the actual foot motion. To compensate for this delay, a number of velocity samples are saved in a temporary data buffer that may be described as a form of first-in first-out (FIFO). When the algorithm indicates the moment to change into the next state, the contents of the FIFO are concatenated to the most recent velocity data. In this manner, the delay that was incurred by Γ_{th} can be eliminated. Another consideration is the size (number of data samples) of the FIFO. This parameter was adjusted by trial-and-error until a satisfactory result was achieved.

In the current implementation of the overall algorithm, there are two dedicated FIFOs. One corresponds to velocity data occurring toward the end of the stance phase. The other FIFO has velocity data from the end of the swing phase. The individual size of each buffer can be adjusted as required. Using the data from these buffers, a complete set of swing phase velocity data can be collected for use in subsequent integration. It is noted that only the velocity data corresponding to the swing phase are integrated to update position. This is based on the assumption that the foot position is fixed during the stance phase.

III. Simulation Results

In this section, simulation results are presented for the adaptive-gain quaternion-based complementary filter and for the position/velocity estimation filter described in the previous section. Experimental results are presented in the section that follows. It should be pointed out that the need for a comprehensive simulation study was prompted by the limitations of the experimental study. The filter performance is simultaneously affected by numerous factors, including sensor calibration errors, thermal effects, magnetic interference, and random measurement error during physical experiments. It can be difficult or impossible to isolate these factors. However, with a well-designed simulation model, the effect of different factors on the filter performance can be individually investigated and analyzed. Additionally, it affords the opportunity to investigate the potential of the filter performance beyond the specifications of presently available sensor modules.

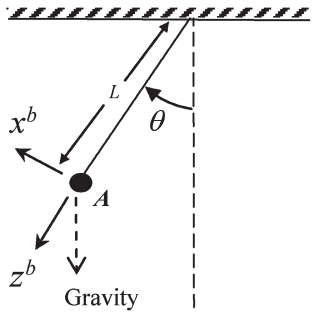

Fig. 7. Schematic of the pendulum used in the simulation study.

A. Simulation Results for an Adjustable Constant-Gain Quaternion-Based Complementary Filter

For evaluation of the performance of the proposed complementary filter through simulation, a model of a vertical pendulum is used [31]. The purpose of this model is to generate data to aid in the study of the performance of the complementary filter during the swing phase of normal walking. In the model, an inertial/magnetic sensor module is assumed to be attached at the swinging end of a pendulum. Theoretical expressions for the sensor data are derived, which model the output of each sensor component when the pendulum is set into motion. In this manner, all of the real-world sensor artifacts, such as gyro bias, accelerometer bias, and motion-induced acceleration, which are understood to influence the orientation estimate, can be controlled and examined.

Fig. 7 shows a pendulum of length L. The angle of the pendulum is denoted by θ, and the positive rotation is in the clockwise direction. A sensor or body coordinate frame is shown in the figure and is denoted by $x^b - y^b - z^b$. An inertial/magnetic sensor module is considered to be attached to point A. The IMMU model has three orthogonally mounted accelerometers, three orthogonally mounted magnetometers, and three orthogonally mounted angular rate sensors. When the accelerometers are subject to pendulum motion, in the absence of noise and misalignment errors, their outputs are characterized by

$$a_x = L\ddot{\theta} + g\,\sin\theta \quad a_y = 0 \quad a_z = -L\dot{\theta}^2 - g\,\cos\theta. \quad (11)$$

In the aforementioned equations, the values of θ, $\dot{\theta}$, and $\ddot{\theta}$ are obtained from a simulation of damped pendulum motion [31]. As for the angular rate sensors, since the pendulum is constrained to swing in the $x^b - z^b$ plane, only the angular rate sensor aligned with the y^b axis senses rotational motion.

As such, the noise-free outputs of the three angular rate sensors are

$$\omega_x = 0 \quad \omega_y = \dot{\theta} \quad \omega_z = 0. \tag{12}$$

The magnetometers measure the earth's magnetic flux density that is projected onto the sensor body axes. Assuming that the plane of the pendulum motion is aligned with magnetic north, the outputs of the magnetometers are given by

$$m_x = |\vec{B}_e|\cos(\beta+\theta) \quad m_y = 0 \quad m_z = |\vec{B}_e|\sin(\beta+\theta) \tag{13}$$

where $\vec{B}_e$ is the earth magnetic flux density vector and β is the angle of inclination. The values for $\vec{B}_e$ and β vary with location, and they were obtained from [32].

The first simulation is designed to validate filter performance while using idealized sensors with no measurement noise. In particular, the angular rate sensors were assumed to be free of any noise or bias. In this case, with the filter gain $k = 0$, the filter is able to perfectly track the pendulum motion. Next, a small sensor error was introduced into the angular rate sensor measurement in the form of a small bias. As expected with a filter gain $k = 0$, the estimated pitch angle tracked the true angle during the first few cycles but began to drift away from the true track toward the end of the motion period. While the errors in the estimated roll and yaw angles were zero in the noiseless case, they grew without bound in the presence of bias errors. The unbounded error with $k = 0$ is the result of relying solely on the integration of angular rate measurements.

Next, the value of k was gradually increased to determine the effect of the FQA on the overall performance of the complementary filter. With the value of k on the order of 50, the unbounded error growth in the estimated roll and yaw angles is capped to a small constant error. However, the estimated pitch angle is unable to track the pendulum motion. This is due to the fact that accelerometers sense not only the acceleration due to gravity but also the centripetal and tangential acceleration of the pendulum. With k set to a relatively high value, the complementary filter relies almost exclusively on accelerometer measurements processed by the FQA. This indicates that a gain value of 50 is too large.

The optimal value of k depends on motions of the pendulum. With a slow-moving pendulum, a large value for k is more appropriate. Conversely, a smaller value for k is more appropriate for a fast-moving pendulum. Fig. 8 shows the output of the complementary filter with $k = 1$ and with the pendulum length L chosen to produce a period of 2 s, corresponding roughly to slow human walking. The estimation error in the pitch angle is less than 1°, and the error in the roll and yaw angles is about 0.1°. The roll and yaw angle errors are due to the presence of angular rate bias introduced into the measurement.

B. Simulation Results of the Adaptive-Gain Position/Velocity Estimation Filter

This section presents a foot motion model for use in simulation of the foot motion tracking algorithm. The algorithm processes simulated sensor data from a foot-mounted inertial/magnetic sensor module. During execution of the simulation, the adaptive-gain complementary filter is used, and its gain switches between two values in response to the stance and swing phases of the simulated foot motion. To simulate foot motion during normal walking, a walking model in the sagittal plane is studied. Although the model in the sagittal plane itself is 2-D, foot motion used for evaluating position/velocity estimation filter is both 2-D and 3-D. Three-dimensional foot motion orthogonal to the sagittal plane results from noise introduced into the sensor model.

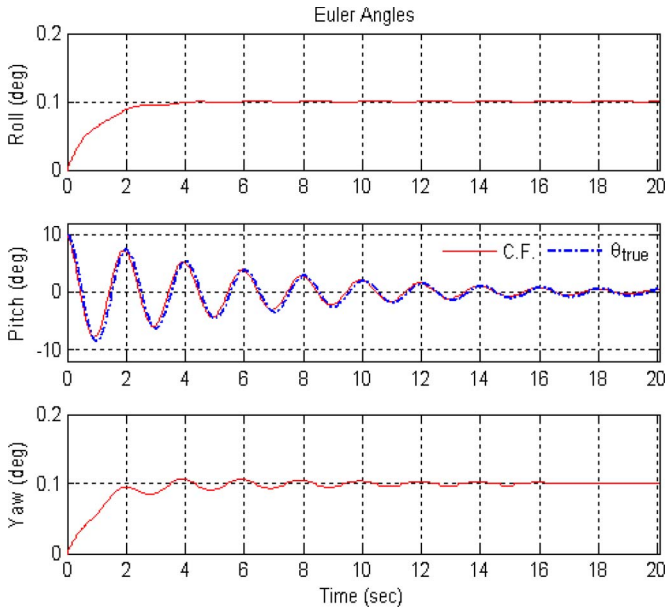

Fig. 8. Complementary filter output (red) and the true pendulum angle (blue) from pendulum simulation with constant gain $k = 1$.

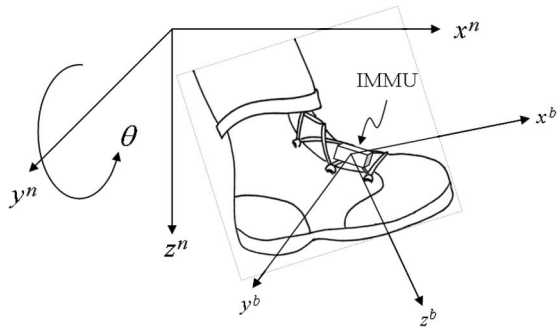

Fig. 9. North–east–down navigation reference frame and the body reference frame attached to the foot.

In the foot simulation, it is assumed that a sensor module is attached to a foot as shown in Fig. 1. Two reference frames are defined as shown in Fig. 9. The north–east–down navigation reference frame $x^n - y^n - z^n$ is stationary, with x^n pointing to the magnetic north, z^n pointing down, and y^n completing the right-hand coordinate system. For simplicity, it is assumed that the sagittal plane is aligned with the $x^n - z^n$ plane and that the foot movement is toward the magnetic north. A body or sensor reference frame $x^b - y^b - z^b$ is attached to the sensor

TABLE I
FOOT MOTION MODEL PARAMETERS

Phase	Subdivision	Duration (sec)	Angular Rate ω_y	Linear acceleration a_x, a_z
Stance phase	Initial contact	0.1	-6.5	0, 0
	Foot flat	0.4	0	0, 0
	Preswing	0.1	-7.5	0, 0
Swing phase	Acceleration	0.2	+3.5	Gaussian
	Deceleration	0.2	+3.5	Gaussian

module, which is attached to the foot. The body reference frame is oriented so that y^b coincides with y^n.

The human gait cycle is divided into two phases: stance phase and swing phase, with the stance phase taking approximately 60% of the gait cycle and the swing phase taking about 40% of the gait cycle [33]. Each phase can be further subdivided, and there are different conventions for doing so. For the purpose of modeling foot motion in this paper, the stance phase is subdivided into three periods, while the swing phase is divided into two periods. The stance phase begins at the moment of *heel strike* and ends at the moment of *toe off*. The *initial contact* period of the stance phase encompasses the length of time from heel strike to foot flat, during which the foot rotates about the heel. The *foot flat* period spans the length of time from the foot flat moment to heel off, during which time the foot is stationary. The *preswing* period covers the length of time from heel off to toe off, during which time the foot rotates about the toe. The swing phase begins at the moment of *toe off* when the toe leaves the ground, continues to *midswing* when the foot passes directly beneath the body, and ends at the moment of *heel strike*. The first time segment from toe off to midswing is characterized by acceleration, and the time period from midswing to heel strike is characterized by deceleration.

Based on the aforementioned discussion, a simplified foot motion model is established, with major attributes summarized in Table I. The total gait cycle is normalized to 1 s, with the stance phase taking 0.6 s and the swing phase taking 0.4 s. For simplicity, the angular velocity ω_y in each of the five periods of the gait cycle is assumed to be a constant. The positive and negative ω_y in the model ensure that the foot attitude returns to its original orientation in preparation for a subsequent foot cycle. The specific values of ω_y in each period chosen in Table I are based on the experimental data collected in this paper and in consultation with the data from [33]. The linear acceleration in the stance phase is zero, and that in the swing phase is discussed in the following.

There are many possible ways to model the acceleration and deceleration that occur during the swing phase, including linear, sinusoidal, Gaussian, and Bezier polynomial models [31]. A comprehensive discussion of all possible models is beyond the scope of the present paper. A Gaussian model, which provides sufficient insight into how to construct other models, is described in more detail in the following discussion.

Foot velocity in the forward direction or x direction during the swing phase has an approximate profile of a bell shape, with rising velocity in the acceleration period of the swing phase and decreasing velocity in the deceleration period. The well-known

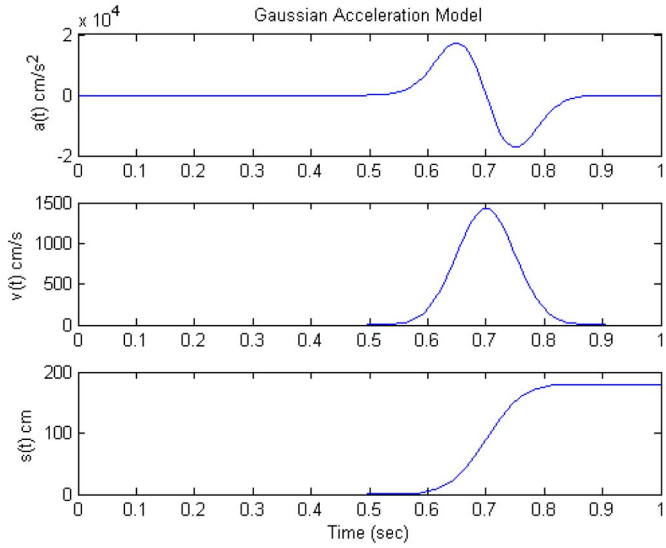

Fig. 10. Forward acceleration, velocity, and position profiles of the Gaussian model for one step.

Gaussian function can be used to model the bell-shaped velocity profile

$$v_x^n(t) = \frac{L_s}{\sigma\sqrt{2\pi}} e^{-t^2/2\sigma^2}, \qquad -\frac{\tau}{2} \le t \le \frac{\tau}{2} \tag{14}$$

where L_s is the stride length, τ is the duration of the swing phase, and $\sigma = 0.05$ is an experimentally determined value that produces a velocity profile similar to those derived from the actual data. The corresponding acceleration is obtained by differentiating (14). Since an analytical expression for the displacement or position is not available, it is instead computed using the MATLAB $erfc()$ function, which is based on a rational Chebyshev approximation of the resulting integral [34]. Fig. 10 shows the forward acceleration, velocity, and position profiles of the Gaussian model.

To model the vertical acceleration of foot motion, it is recognized that the net vertical displacement returns to zero for normal walking on level surfaces. With this in mind, a Gaussian model is adopted for the vertical position

$$p_z^n(t) = \frac{M_s}{\sigma\sqrt{2\pi}} e^{-t^2/2\sigma^2}, \qquad -\frac{\tau}{2} \le t \le \frac{\tau}{2} \tag{15}$$

where M_s is chosen such that $M_s/\sigma\sqrt{2\pi}$ is equal to the maximum vertical displacement of the foot in the swing phase. The corresponding vertical velocity and acceleration are obtained by differentiation. By assuming a sagittal plane model, the position, velocity, and acceleration in the y direction are zero.

Using the simplified foot motion model in the sagittal plane, the sensor measurements for accelerometers, magnetometers, and angular rate sensors can be generated. First, the foot pitch angle θ is derived from the angular rate model for each of the five periods in Table I. The corresponding quaternion representing the foot orientation is given by

$$q = [q_0\ q_1\ q_2\ q_3] = \left[\cos\frac{\theta}{2}\ 0\ \sin\frac{\theta}{2}\ 0\right]. \tag{16}$$

Second, the acceleration measurement provided by the sensor module is in the body reference frame, whereas the foot acceleration model described in the preceding paragraphs is in the navigation reference frame. As such, the acceleration measurement is obtained by converting the modeled acceleration in the navigation reference frame into the body reference frame

$$a^b = q^*(a^n + g^n)q. \tag{17}$$

In the previous discussion, it is noted that the gravitational acceleration is added.

Third, the magnetometer measurements are constructed using the foot pitch angle. The expressions for the magnetometers have the same form as those used for the pendulum motion in (13). Based on the foot motion model, noise-free measurements of accelerometers, magnetometers, and angular rate sensors are generated as described previously.

To simulate a real-world sensor measurement, a noise model is introduced so that its impact on the filter performance can be investigated. In the MATLAB simulation, the noise is modeled as

$$\mu + \sigma\ randn(\cdot) \tag{18}$$

where $randn()$ is the random number generator that produces samples having a Gaussian distribution, μ is the mean value of the noise, and σ is the standard deviation. The mean value μ represents bias in the sensor measurement due to calibration error, null-bias error, scale-factor error, cross-axis coupling error, etc. The standard deviation σ models the magnitude of random noise in the sensor measurements.

To identify suitable values of μ and σ for the noise model (18), the measured statistics of the actual IMMU were considered, as well as the manufacturer's specification sheet. A MicroStrain 3DM-GX1 sensor module was placed on a stationary surface for 1 h and 35 min. Approximately 297 000 data samples were collected from each of the accelerometers, magnetometers, and angular rate sensors. Fig. 11 shows the power spectral density (PSD) for one of the accelerometers. The PSD was computed using the MATLAB function $cpsd()$. The upper plot is the PSD of the actual measurement data, while the lower plot is the PSD of the simulated noise generated using (18), with $\mu = 0.0021$ and $\sigma = 0.0033$, which were determined from the actual measurement data. It should be noted that accelerometer bias cannot be determined reliably due to the presence of gravity. The value of μ in this case is determined from the measurement data of the sensor module under a specific condition and is not representative. Its purpose is to show the effectiveness of the noise model in representing the actual sensor noise. The actual value of μ used in the simulation is discussed later in this section. It is seen that the two plots are similar, suggesting that the noise model (18) is suitable for modeling sensor noise. Reading from the upper plot, the accelerometer noise power is approximately -65 dBG^2/Hz, or equivalently 562 μG/$\sqrt{\text{Hz}}$. This value compares favorably with the specification value of 400 μG/$\sqrt{\text{Hz}}$ for the 3DM-GX1.

Similarly, the noise power level for the angular rate sensors is found to be approximately -57 dB(rad/sec)^2/Hz, which is converted to an equivalent value of 4. 85 deg/$\sqrt{\text{hr}}$. Again, this

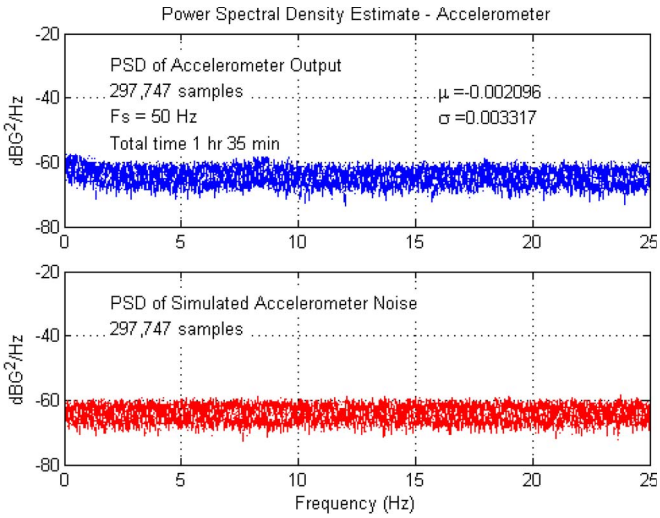

Fig. 11. PSD of (upper plot) measured accelerometer output and (lower plot) simulated accelerometer noise model.

value compares reasonably with the manufacturer's specification of 3. 5 deg/$\sqrt{\text{hr}}$. The corresponding mean and standard deviation measured from the actual sensor output are $\mu = 7.25 \times 10^{-6}$ and $\sigma = 0.0076$.

The noise power for the magnetometers is approximately -75 dB(gauss)^2/Hz. Since the manufacturer specification sheet does not provide a noise power density for the magnetometer, a comparison cannot be made. The mean and standard deviation for the measured magnetometer noise are $\mu = 0.15$ and $\sigma = 0.00082$.

It is noted that the random noise standard deviation σ and the bias μ for the angular rate sensor can be adequately determined based on the static experiment as described previously. This is because angular rate sensors have zero input while they are stationary. However, accelerometers and magnetometers are under the inescapable influence of gravity and the magnetic field of the earth, respectively. As such, the bias for these sensors cannot be determined from a static experiment. Therefore, the noise models for accelerometer and magnetometer use the measured σ and an estimated μ based on the sensor specification.

From the 3DM-GX1 data sheet, accelerometer bias is ± 0.005 g, with a measurement range of ± 5.0 g. In simulation, a bias of 0.1% full scale is selected for the accelerometer and magnetometer. All of the noise model parameters, as well as other simulation parameters, are summarized in Table II. It is to be understood that these noise parameters are used as base parameters. When investigating the effect of noise on the filter performance, these base parameters are scaled up or down in the simulation to observe the resulting overall impact.

To begin the examination of the position estimation filter, walking motion with noise-free sensor data is considered first, followed by introducing noise in various combinations. The simulation results presented in the following are for a 100-step straight walk in the north direction. The first set of simulations is conducted to evaluate the effect of random noise in the absence of sensor bias. The sensor bias is set to zero ($\mu = 0$), and the standard deviation σ of random noise is scaled from its base

TABLE II
SENSOR NOISE AND OTHER SIMULATION PARAMETERS

Sensor noise parameters	Accelerometer error	$\mu = 0.1\%$ of full scale $\sigma = 0.033$ m/s^2
	Magnetometer error	$\mu = 0.1\%$ of full scale $\sigma = 0.82\times10^{-3}$ Gauss
	Angular rate sensor error	$\mu = 7.25\times10^{-6}$ rad/s $\sigma = 0.0076$ rad/s
Simulation parameters	Stride length	1.2 m
	Vertical displacement	0.25 m
	Sampling frequency	50 Hz
Adaptive gain values	Static gain	$k_s = 1.05$
	Dynamic gain	$k_d = 0.0$

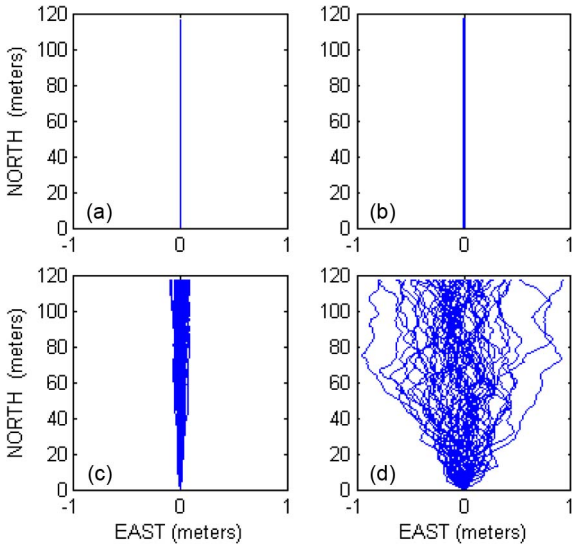

Fig. 12. Simulation results for fifty 100-step straight-line walks. (a) No sensor error and sensor error scale factor equal to (b) 0.1, (c) 1.0, and (d) 10.0 (units of the horizontal and vertical axes do not have a one-to-one correspondence in size).

value to lower and higher values. Fig. 12 shows the simulation results of the position estimation filter, in which each plot shows the estimated walking trajectories of 50 simulations in order to gain some sense of the statistics. Fig. 12(a) shows the noise-free result. As expected, the walking trajectory is a straight line in the direction of true north. Fig. 12(b)–(d) shows the result with the random noise σ scaled by 0.1, 1.0, and 10.0 from its base value, respectively. As the sensor noise is increased, there is a corresponding increase in the resulting position error. The spread of the end position error in the east/west direction can be easily seen from the figure. In particular, the maximum position error in the east/west direction is about 1 m when the random noise is scaled by 10.0 from the base value. The results from this simulation indicate that the random noise component of sensor error has relatively small impact on filter performance. When the random noise σ is scaled by 1.0, i.e., when the same amount of random noise present in the MicroStrain 3DM-GX1 is used in the simulation, the position error is less than 0.1% of the total walked distance.

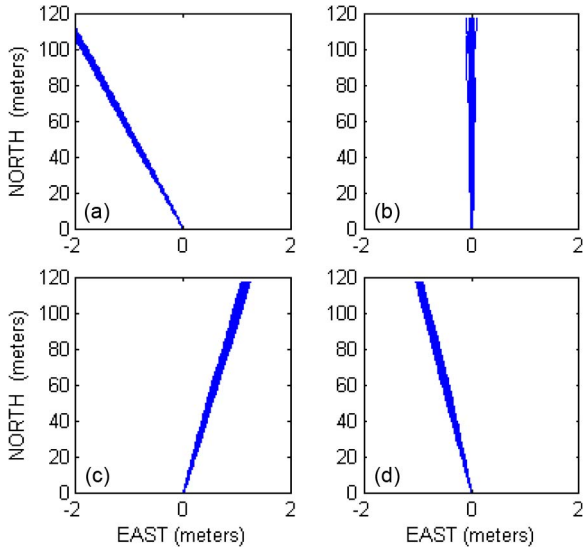

Fig. 13. Simulation results for fifty 100-step straight-line walks with sensor error scale factor equal to one and (a) accelerometer bias only, (b) angular rate sensor bias only, (c) magnetometer bias only, and (d) all sensor biases included (units of the horizontal and vertical axes do not have a one-to-one correspondence in size).

It is noted that these results were obtained using the adaptive-gain approach for the complementary filter. The filter gain switches between two values listed in Table II. If a constant gain value was used for the complementary filter, the performance of the position estimation algorithm was severely degraded. As an example, when a constant gain of 1.0 was used, the position error was 13.6% of the total walked distance.

Next, the effect of sensor bias on the filter performance is studied. The bias in accelerometers, angular rate sensors, and magnetometers is first introduced individually, and then, biases for all three sensor types are included. The base bias values listed in Table II are used. At the same time, an amount of the random noise scaled by 1.0 is also included in the corresponding sensor. The simulation results are shown in Fig. 13. Fig. 13(a) shows the result when only the accelerometer bias is introduced, Fig. 13(b) shows that of the angular rate bias only, and Fig. 13(c) shows that of the magnetometer bias only. Finally, Fig. 13(d) shows the simulation result when all sensor biases are included. It is clearly seen that the spread of the position error in the east/west direction is similar in magnitude to that of Fig. 12(c). However, the inclusion of sensor bias causes the estimated position to drift in one direction.

The simulation of the position/velocity estimation filter was described previously. Based on a foot motion model and sensor noise model, simulated sensor measurements are generated and used to evaluate the position/velocity estimation filter. The simulation study offers the flexibility of investigating the effect of various sensor noise sources individually or simultaneously as reported in this section. It can also be used to easily investigate the effect of sampling rates and numerical integration methods [31]. From the results presented previously, it becomes evident that sensor biases have significantly more impact on the estimated walking position than random noise. Biases in accelerometers, magnetometers, and angular rate sensors all tend to introduce an unbounded drift in the estimated position.

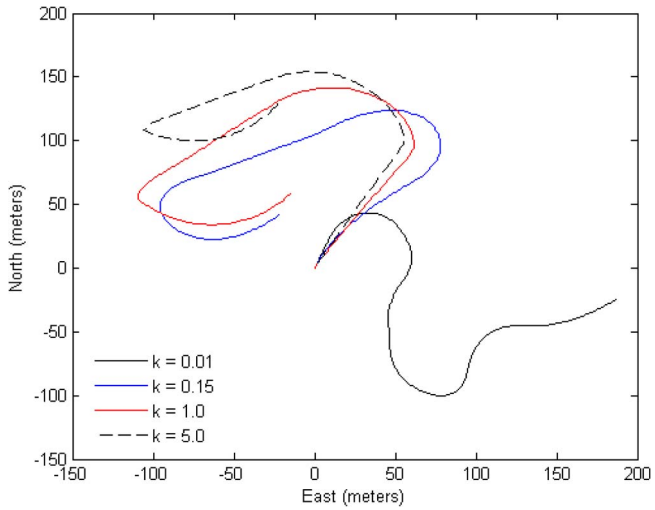

Fig. 14. Estimated walking position trajectory using a constant-gain complementary filter.

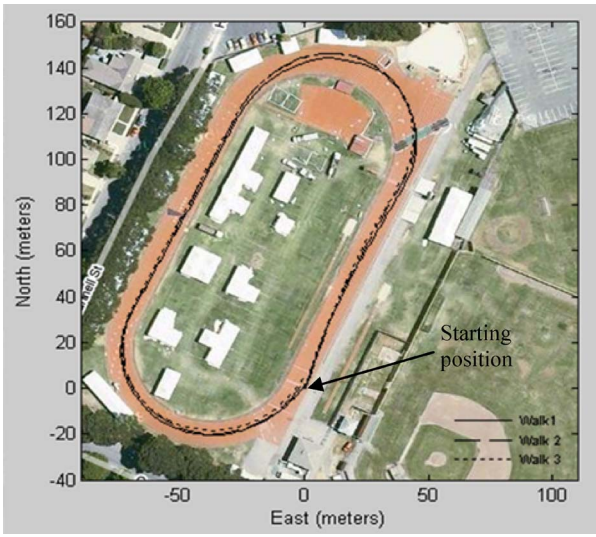

Fig. 15. Estimated walking trajectories overlaid onto Google map of the athletic track field. Adaptive-gain strategy was used for the complementary filter gains.

IV. Experimentation

In this section, experimental walking results conducted on an athletic track field are first presented. Then, the optimal selection of filter gains with respect to the estimation accuracy is discussed. Finally, some remarks on the simulation and experimental results are provided.

A. Experimental Results

The experimental system consists of a MicroStrain 3DM-GX1 sensor module attached to the foot as shown in Fig. 1 and a Sony UXP-180 minicomputer carried in a backpack for data acquisition. The experiment was conducted on a standard athletic track field. The circumference of the innermost lane is 400 m. Lane 7, where the experimental walks took place, has a length of 437.50 m. All walks were conducted in a counterclockwise direction and began and ended at the same point on the track. Multiple walks were conducted. All sensor data were logged and processed afterward using MATLAB.

In the first experiment, the complementary filter gain was set to a constant value throughout the entire walk. Fig. 14 shows the position estimation results for four gain values $k = 0.01,\ 0.15,\ 1.0,$ and 5.0. Upon inspection of the plot, it is seen immediately that the second gain value $(k = 0.15)$ produces a position trajectory (the blue line in Fig. 14) that somewhat resembles the oval path of the athletic track. When a smaller or larger gain value is used, the tracking result becomes worse. In particular, when $k = 0.01$, the estimated position drifted in a direction away from the oval path.

In the next experiment, an adaptive-gain strategy is utilized in the complementary filter. The filter gain is switched between two values according to the output of the gait phase detection algorithm. When the foot is in the stance phase, the gain is set to a nominally high value. This is where the motion-induced accelerations are lower, and the FQA produces better results. During the swing phase, the foot is moving through the air, experiencing rapidly changing acceleration, and the filter gain is set to a low value such that more of the dynamic quaternion is represented in the filter output. Fig. 15 shows the estimated position for the three walks around the athletic track overlaid onto a satellite image of the actual track. Qualitatively, these tracks represent a marked improvement over those computed using the constant-gain filter (compare with previous figure). The overall shape and orientation of the computed tracks appear very similar to the athletic track shown in the same figure. The quantitative measure of the filter performance is summarized in Table III.

TABLE III
Experimental Performance of the Adaptive-Gain Complementary Filter

	Distance (m)	Distance Error	ΔXY (m)	% Error of Walked Distance
Walk 1	438.43	0.21%	2.52	0.58%
Walk 2	439.30	0.41%	3.37	0.77%
Walk 3	438.35	0.19%	4.84	1.10%

The percentage of distance error reported in the third column is calculated from the walking distance estimated by the filter and the reference distance of the track (437.50 m). The average of the distance errors from three experimental walks is 0.27%. Another measure of the filter performance is shown in the last two columns. All actual walks start and end at the same position. The fourth column ΔXY reports the radial distance from the start position to the end position estimated by the filter. The last column shows this radial distance as a percentage of the walked distance. These experimental results demonstrate that the complementary filter with adaptive gain is highly effective in providing accurate distance as well as position estimation. The accuracy for the position estimation is on the order of 1% of the distance walked. This result compares favorably with those reported in the literature (e.g., the position accuracy of 0.3% reported in [19] and 2.0% reported in [20]), although

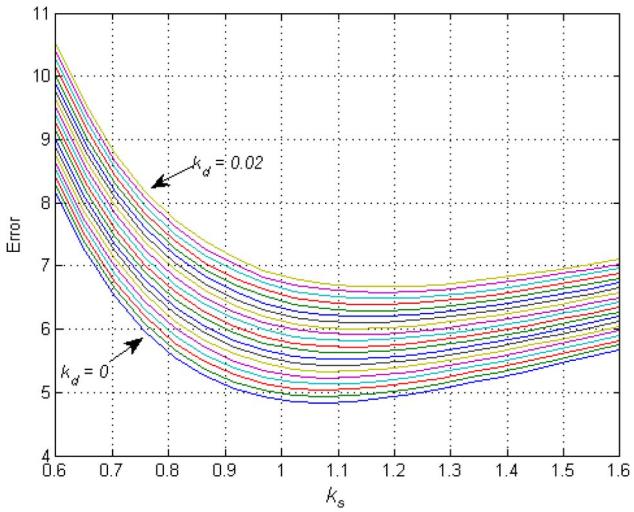

Fig. 16. Optimization curves for different values of the dynamic gain k_d. The vertical axis is the ΔXY error that serves as a cost function for the optimization problem.

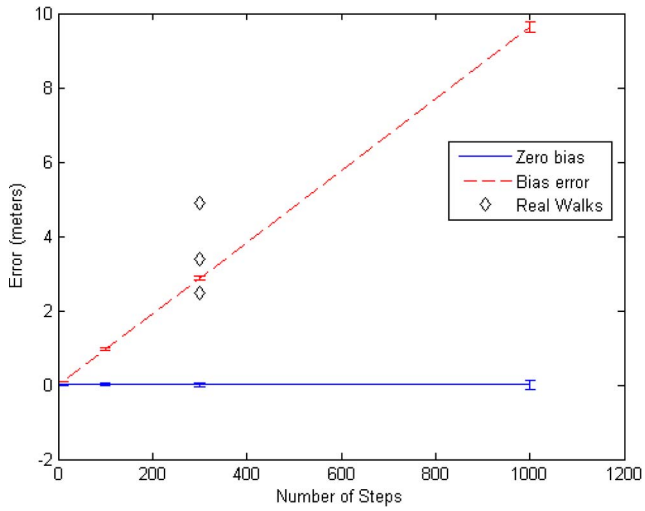

Fig. 17. Comparison of the position errors in the east/west direction from the simulation and experiment. The vertical axis is the ΔXY error.

completely different sensor modules were used in respective experiments. The average distance error of 0.27% indicates that position error could be improved with better calibration of the magnetometers.

The following section provides more insight into the selection of gain values in the complementary filter.

B. Filter Gain Selection

In the adaptive-gain complementary filter, two gain values are used: static gain k_s and dynamic gain k_d. The former is used when the accelerations are low, as in the stance phase of the foot motion, while the latter is used during the swing phase, when the motion is high. To determine the two filter gain values that produce the best result, a simple optimization study was accomplished using the sensor data from one of the actual walks around the athletic track. The sensor data were processed with the navigation algorithm (Fig. 2), and a pair of gain values k_s and k_d was selected from a range of gains under consideration. The position error ΔXY resulting from this particular pair of gain values was noted. Next, another iteration of the navigation algorithm was accomplished using a new pair of gains, again noting the resulting ΔXY. This was continued until the entire range of k_s and k_d under consideration had been exhausted. In Fig. 16, the pair of gain values that gave the smallest ΔXY error was then selected. In this fashion, the filter gains k_s and k_d were optimized for the experimental data.

From this paper, it is determined that, for walking motion, setting the filter gain to zero $(k_d = 0)$ during the swing phase produces the best results. During the swing phase, the foot acceleration changes very rapidly. As a result, the FQA gives large errors during this phase of the foot motion. In spite of the angular rate sensor biases and its associated error, it is still better to rely entirely on angular rate measurements rather than accelerometer measurements during the swing phase.

During the stance phase, when the motion-induced accelerations are lower, it is beneficial to have a larger component of the filter output derived from the FQA. Setting $k_s = 1.05$ during this period of the walking motion gives good results. However, as shown in the plot, a value larger than this is not desirable because the error is seen to increase. This is possibly due to the fact that, during the stance phase of normal walking, the foot translational velocity is zero, while its angular velocity is not. In this phase, the foot is rotating from the heel to the toe in preparation for the next step. If we compare this motion to that of the pendulum, then the foot will experience some normal and tangential acceleration that will affect the overall accelerometer output. Thus, the optimization shows that, for this phase of walking motion, it is better to have a blended filter output consisting of both the dynamic and static components.

C. Discussion

In the simulation study, it was revealed that sensor biases seem to be the principal source of the position estimation error. Experimental results tend to support this conclusion as well. The correlation between the simulation and experimental results is shown in Fig. 17. The sloped red line is the mean of the position error in the east/west direction predicted by the simulation as a function of the number of walking steps. The variances at 50, 300, and 1000 steps are annotated by two horizontal bars. The three diamonds indicate the position error from three real 300-step walks. The proximity of the experimental data to the bias simulation suggests that a larger part of position error may be a result of sensor biases.

Additionally, it is noteworthy to closely examine the end position of the three walks conducted on the athletic track field as shown in Fig. 18. The estimated end positions of all three walks are clustered in one area to the north of the starting position. Although three data points are not necessarily of statistical significance, they nevertheless suggest that, for the sensors that we had, available biases (rather than random noise) are likely the main source of the position estimation error.

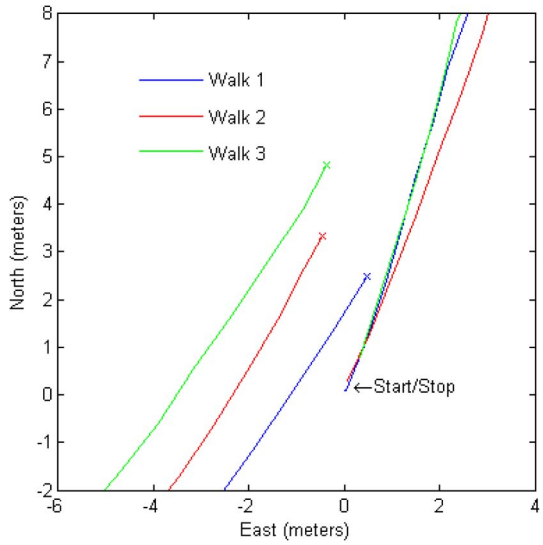

Fig. 18. Close-up of the starting position and end positions of the three walks around the athletic track.

V. Conclusion

A. Summary

This paper has described an algorithm for estimating human foot position during normal walking based on estimates of foot orientation, velocity, acceleration, and gait phase using inertial/magnetic sensor measurements. The measurements are provided by an IMMU attached to a foot. Orientation estimation is accomplished by a quaternion-based complementary filter that uses a variable scalar gain factor to blend the high-frequency information provided by angular rate sensors and the low-frequency information provided by accelerometers and magnetometers. Although presented in the context of the foot motion estimation, the complementary orientation filter can be used to track orientation of any other object to which the IMMU is attached. The filter gain can be adaptively adjusted based on the intended application. For the foot motion estimation, it is shown that a two-value switch strategy is effective. The switch strategy selects a lower value dynamic gain during the swing phase and a higher value static gain during the stance phase of the foot motion. For this purpose, a foot gait phase detection algorithm based on the use of angular rate sensor measurements was also presented.

Foot acceleration is directly measured by the accelerometers of the IMMU. However, the measurements are represented in the sensor or body coordinate frame. For many applications, it is desirable to have foot acceleration in the earth coordinate frame. With foot orientation readily available as a result of the quaternion-based complementary filter, foot acceleration in the body coordinate frame is conveniently converted into the earth coordinate frame using the foot orientation quaternion.

Foot velocity is obtained by numerically integrating corrected foot acceleration measurements obtained during the swing phase. Due to sensor noise, accelerometer measurements tend to drift. The drift is corrected using the ZVU technique, which is based on the fact that foot velocity is known to be zero during stance phases. The corrected foot velocity is integrated to obtain foot position.

Simulations and experiments were conducted to evaluate the algorithm. The experimental results suggest that the achievable position accuracy of the algorithm is about 1% of the total walked distance. The simulation study suggests that sensor biases are the main source of the position error.

B. Future Work

A focus of future work will be to explore calibration techniques beyond those performed in a laboratory setting. Such techniques might include some preliminary measurements with the sensor installed in its intended field of use, thereby providing a sort of *in situ* calibration. The calibration method for three-axis accelerometers and magnetometers described in [35] will be considered because it only involves arbitrary rotations of sensor modules without the need of special calibration equipment.

Sensor calibration and the precision with which it can be determined are an essential component of the overall system performance. Further study is required here to assess the limits of calibration precision of MEMS-based sensor technology and evaluation of other sensor architectures when they are available.

A main component of our ongoing work is to assess the extensibility of this approach to a larger group of people and to determine the sensitivities of the various parameters utilized within the algorithm. The filter gains of the complementary filter and the tuning parameters within the gait phase detection algorithm should be examined in terms of their influence on the overall performance when the larger user group is considered.

References

[1] D. Roetenberg, P. J. Slycke, and P. H. Veltink, "Ambulatory position and orientation tracking fusing magnetic and inertial sensing," *IEEE Trans. Biomed. Eng.*, vol. 54, no. 5, pp. 883–890, May 2007.
[2] D. G. M. Zwartjes, T. Heida, J. P. P. van Vugt, J. A. G. Geelen, and P. H. Veltink, "Ambulatory monitoring of activities and motor symptoms in Parkinson's disease," *IEEE Trans. Biomed. Eng.*, vol. 57, no. 11, pp. 2778–2786, Nov. 2010.
[3] I. Tien, S. D. Glaser, R. Bajcsy, D. S. Goodin, and M. J. Aminoff, "Results of using a wireless inertial measuring system to quantify gait motions in control subjects," *IEEE Trans. Inf. Technol. Biomed.*, vol. 14, no. 4, pp. 904–915, Jul. 2010.
[4] [Online]. Available: www.intersense.com
[5] [Online]. Available: www.xsens.com
[6] [Online]. Available: www.microstrain.com
[7] [Online]. Available: www.memsense.com
[8] C. T. Judd, "A personal dead reckoning module," in *Proc. ION GPS*, Kansas City, MO, Sep. 1997, pp. 47–51.
[9] S. E. Crouter, P. L. Schneider, M. Karabulut, and D. R. Bassett, Jr., "Validity of 10 electronic pedometers for measuring steps, distance, and energy cost," *Med. Sci. Sports Exerc.*, vol. 35, no. 8, pp. 1455–1460, Aug. 2003.
[10] Q. Ladetto and B. Merminod, "In step with GPS," *GPS World*, vol. 10, no. 10, pp. 30–38, Oct. 2002.
[11] C. Randell, C. Djiallis, and H. Muller, "Personal position measurement using dead reckoning," in *Proc. 7th IEEE Int. Symp. Wearable Comput.*, Oct. 18–21, 2003, pp. 166–173.
[12] S. W. Lee and K. Mase, "Activity and location recognition using wearable sensors," *IEEE Pervasive Comput.*, vol. 1, no. 3, pp. 24–32, Jul.–Sep. 2002.
[13] C. Toth, D. A. Grejner-Brzezinska, and S. Moafipoor, "Pedestrian tracking and navigation using neural networks and fuzzy logic," in *Proc. Int. Symp. Intell. Signal Process. WISP*, Oct. 3–5, 2007, pp. 1–6.
[14] J. Elwell, "Inertial navigation for the urban warrior," in *Proc. SPIE Conf. Digitization Battlespace IV*, Orlando, FL, Apr. 7/8, 1999, vol. 3709, pp. 196–204.

[15] K. Sagawa, Y. Satoh, and H. Inooka, "Non-restricted measurement of walking distance," in *Proc. IEEE Int. Conf. Syst., Man, Cybern.*, Nashville, TN, Oct. 2000, vol. 3, pp. 1847–1852.
[16] A. M. Sabatini, C. Martelloni, S. Scapellato, and F. Cavallo, "Assessment of walking features from foot inertial sensing," *IEEE Trans. Biomed. Eng.*, vol. 52, no. 3, pp. 486–494, Mar. 2005.
[17] F. Cavallo, A. M. Sabatini, and V. Genovese, "A step toward GPS/INS personal navigation systems: Real-time assessment of gait by foot inertial sensing," in *Proc. IEEE/RSJ Int. Conf. IROS*, Edmonton, AB, Canada, Aug. 2005, pp. 1187–1191.
[18] A. M. Sabatini, "Quaternion-based extended Kalman filter for determining orientation by inertial and magnetic sensing," *IEEE Trans. Biomed. Eng.*, vol. 53, no. 7, pp. 1346–1356, Jul. 2006.
[19] E. Foxlin, "Pedestrian tracking with shoe-mounted inertial sensors," *IEEE Comput. Graph. Appl.*, vol. 25, no. 6, pp. 38–46, Nov./Dec. 2005.
[20] L. Ojeda and J. Borenstein, "Personal dead-reckoning system for GPS-denied environments," in *Proc. IEEE Int. Workshop SSRR*, Sep. 27–29, 2007, pp. 1–6.
[21] O. Bebek, M. A. Suster, S. Rajgopal, M. J. Fu, X. Huang, M. C. Cavusoglu, D. J. Young, M. Mehregany, A. J. van den Bogert, and C. H. Mastrangelo, "Personal navigation via high-resolution gait-corrected inertial measurement units," *IEEE Trans. Instrum. Meas.*, vol. 59, no. 11, pp. 3018–3027, Nov. 2010.
[22] C. Zhou, J. Downey, D. Stancil, and T. Mukherjee, "A low-power shoe-embedded radar for aiding pedestrian inertial navigation," *IEEE Trans. Microw. Theory Tech.*, vol. 58, no. 10, pp. 2521–2528, Oct. 2010.
[23] I. P. I. Pappas, M. R. Popovic, T. Keller, V. Dietz, and M. Morari, "A reliable gait phase detection system," *IEEE Trans. Neural Syst. Rehabil. Eng.*, vol. 9, no. 2, pp. 113–125, Jun. 2001.
[24] H. M. Schepers, H. F. J. M. Koopman, and P. H. Veltink, "Ambulatory assessment of ankle and foot dynamics," *IEEE Trans. Biomed. Eng.*, vol. 54, no. 5, pp. 895–902, May 2007.
[25] R. G. Brown and P. Y. C. Hwang, *Introduction to Random Signals and Applied Kalman Filtering*, 3rd ed. New York: Wiley, 1996.
[26] X. Yun, E. R. Bachmann, and R. B. McGhee, "A simplified quaternion-based algorithm for orientation estimation from earth gravity and magnetic field measurements," *IEEE Trans. Instrum. Meas.*, vol. 57, no. 3, pp. 638–650, Mar. 2008.
[27] J. B. Kuipers, *Quaternions and Rotation Sequences*. Princeton, NJ: Princeton Univ. Press, 1999.
[28] J. Calusdian, X. Yun, and E. Bachmann, "Adaptive-gain complementary filter of inertial and magnetic data for orientation estimation," in *Proc. IEEE Int. Conf. Robot. Autom.*, Shanghai, China, May 2011, pp. 1916–1922.
[29] A. Winter, *Biomechanics and Motor Control of Human Movement*, 3rd ed. Hoboken, NJ: Wiley, 2005.
[30] I. Skog, P. Handel, J. O. Nilsson, and J. Rantakokko, "Zero-velocity detection—An algorithm evaluation," *IEEE Trans. Biomed. Eng.*, vol. 57, no. 11, pp. 2657–2666, Nov. 2010.
[31] J. Calusdian, "A personal navigation system based on inertial and magnetic field measurements," Ph.D. dissertation, Naval Postgraduate School, Monterey, CA, Sep. 2010.
[32] National Oceanic and Atmospheric Administration, United States Department of Commerce. [Online]. Available: http://www.noaa.gov/
[33] P. K. Levangie and C. C. Norkin, *Joint Structure and Function*. Philadelphia, PA: F.A. Davis Comp., 2001.
[34] W. J. Cody, "Rational Chebyshev approximations for the error function," *Math. Comput.*, vol. 23, no. 107, pp. 631–637, Jul. 1969.
[35] F. Camps, S. Harasse, and A. Monin, "Numerical calibration for 3-axis accelerometers and magnetometers," in *Proc. IEEE Int. Conf. Electro/Inf. Technol.*, Windsor, ON, Canada, Jun. 7–9, 2009, pp. 217–221.

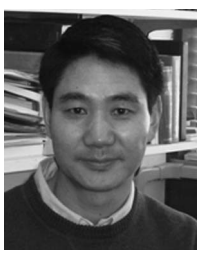

Xiaoping Yun (S'86–M'87–SM'96–F'05) received the B.S. degree from Northeastern University, Shenyang, China, in 1982 and the M.S. and D.Sc. degrees from Washington University, St. Louis, MO, in 1984 and 1987, respectively.

He is currently a Distinguished Professor of electrical and computer engineering with the Naval Postgraduate School, Monterey, CA. His research interests include coordinated control of multiple robotic manipulators, mobile manipulators, mobile robots, control of nonholonomic systems, microelectromechanical system sensors, inertial navigation, virtual environments, and human body motion tracking using inertial/magnetic sensors.

Prof. Yun was an Associate Editor of the IEEE TRANSACTIONS ON ROBOTICS AND AUTOMATION from 1993 to 1996 and a Coeditor of the special issue on mobile robots of the IEEE ROBOTICS AND AUTOMATION MAGAZINE in 1995. He was a Cochair of the RAS Technical Committee on Mobile Robots in 1992–2003, a member of the RAS Conference Board in 1999–2007, a member of the Program Committee of the IEEE International Conference on Robotics and Automation in 1990, 1991, 1997, 1999, 2000, 2003, and 2004, a member of the Program Committee of IEEE/RSJ International Conference on Intelligent Robots and Systems in 1998, 2001, 2003, and 2004, the General Cochair of the 1999 IEEE International Symposium on Computational Intelligence in Robotics and Automation, the Finance Chair of the IEEE International Conference on Robotics and Automation in 2002 and 2004, the Finance Chair of the IEEE/RSJ International Conference on Intelligent Robots and Systems in 2001, 2004, 2005, 2006, and 2011, the Finance Chair of the IEEE International Conference on Nanotechnology in 2001, and the General Chair of the IEEE Nanotechnology Materials and Devices Conference in 2010. He is the Treasurer of the IEEE Robotics and Automation Society in 2004–2011 and the Vice President for Finance of the IEEE Nanotechnology Council in 2004–2006 and 2011–2012. He was the Vice President for Publications of the IEEE Nanotechnology Council in 2010.

James Calusdian received the B.S. degree in electrical engineering from California State University, Fresno, in 1989 and the M.S. and Ph.D. degrees in electrical engineering from the Naval Postgraduate School, Monterey, CA, in 1998 and 2010, respectively.

He began his professional career at the Air Force Flight Test Center, Edwards Air Force Base, CA, where he worked on flight test instrumentation systems on various types of aircraft. He also worked as a Flight Test Engineer supporting test and evaluation of developmental aircraft systems. Since 2001, he has been with the Naval Postgraduate School as the Director of the Control Systems Laboratory and the Optical Electronics Laboratory. His interests include inertial and magnetic sensor integration/applications, embedded system applications/programming, and optical electronics.

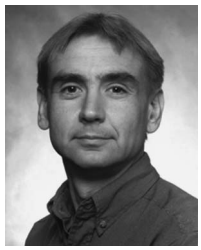

Eric R. Bachmann (M'01) received the B.S. degree from the University of Cincinnati, Cincinnati, OH, and the M.S. and Ph.D. degrees from the Naval Postgraduate School, Monterey, CA.

He holds positions as an Associate Professor with Miami University, Oxford, OH, and as a Research Assistant Professor with the Naval Postgraduate School, Monterey, CA. Prior to this, he was an officer and an unrestricted naval aviator with the U.S. Navy. His research interests include virtual environments as well as posture and position tracking.

Robert B. McGhee (M'58–SM'85–F'90–LF'94) was born in Detroit, MI, in 1929. He received the B.S. degree in engineering physics from the University of Michigan, Ann Arbor, in 1952 and the M.S. and Ph.D. degrees in electrical engineering from the University of Southern California, Los Angeles, in 1957 and 1963, respectively.

From 1952 to 1955, he served on active duty as Guided Missile Maintenance Officer with the U.S. Army Ordnance Corps. From 1955 to 1963, he was a member of the technical staff of Hughes Aircraft Company, Culver City, CA, where he worked on guided missile simulation and control problems. In 1963, he joined the Department of Electrical Engineering, University of Southern California, as an Assistant Professor. He was promoted to Associate Professor in 1967. In 1968, he was appointed as a Professor of electrical engineering and the Director of the Digital Systems Laboratory, Ohio State University, Columbus. In 1986, he joined the Computer Science Department, Naval Postgraduate School, Monterey, CA, where he served as the Department Chair from 1988 to 1992. Subsequently, he held the position of Professor of computer science until his retirement in 2004. He now serves as Emeritus Professor and continues his involvement in ongoing research in human motion tracking, mission control for autonomous vehicles, and related topics.